Two-dimensional direct numerical simulation of spray flames - Part 1: Effects of equivalence ratio, fuel droplet size and radiation, and validity of flamelet model

AUTHOR(S):

Fujita, Akitoshi; Watanabe, Hiroaki; Kurose, Ryoichi; Komori, Satoru

CITATION:

Fujita, Akitoshi ...[et al]. Two-dimensional direct numerical simulation of spray flames - Part 1: Effects of equivalence ratio, fuel droplet size and radiation, and validity of flamelet model. Fuel 2013, 104: 515-525

ISSUE DATE:

2013-02

URL:

http://hdl.handle.net/2433/166086

Two-dimensional direct numerical simulation of spray flames. Part 1: Effects of equivalence ratio, fuel droplet size and radiation, and validity of flamelet model

Akitoshi Fujita[a], Hiroaki Watanabe[b], Ryoichi Kurose[*,a], Satoru Komori[a]

[a] *Department of Mechanical Engineering and Science, and Advanced Research Institute of Fluid Science and Engineering, Kyoto University, Yoshida-honmachi, Sakyo-ku, Kyoto, Kyoto 606-8501, Japan*

[b] *Energy Engineering Research Laboratory, Central Research Institute of Electric Power Industry (CRIEPI), 2-6-1 Nagasaka, Yokosuka, Kanagawa 240-0196, Japan*

Abstract

The effects of equivalence ratio, fuel droplet size, and radiation on jet spray flame are investigated by means of two-dimensional direct numerical simulation (DNS). In addition, the validity of an extended flamelet/progress-variable approach (EFPV), in which heat transfer between droplets and ambient fluid including radiation is exactly taken into account, is examined. n-decane ($C_{10}H_{22}$) is used as liquid spray fuel, and the evaporating droplets' motions are tracked by the Lagrangian method. The radiative heat transfer is calculated using the discrete ordinate method with S_8 quadrature approximation. The results show that the behavior of jet spray flame is strongly affected by equivalence ratio and fuel droplet size. The general behavior of the jet spray flames including the heat transfer between droplets and ambient fluid with radiation effect can be captured by EFPV.

Key words: Numerical simulation; Spray combustion; Jet flame; Radiation; Flamelet model

*Corresponding author. fax: +81 75 753 9218.
Email address: kurose@mech.kyoto-u.ac.jp (Ryoichi Kurose)

1. Introduction

Spray combustion is utilized in a number of engineering applications such as energy conversion and propulsion devices. It is therefore necessary to predict the spray combustion behavior precisely when designing and operating equipment. However, since spray combustion is a complex phenomenon in which the dispersion of the liquid fuel droplets, their evaporation, and the chemical reaction of the fuel vapor with the oxidizer take place interactively at the same time, the underlying physics governing these processes has not been well understood.

Recently, the spray combustion behavior has been studied by direct numerical simulations (DNS) [e.g., 1-8] or large-eddy simulations (LES) [e.g., 9-12]. However, since these computations are still so expensive that the effects of the changes in combustion conditions such as equivalence ratio, fuel droplet size and ambient pressure on the spray combustion behavior have not been sufficiently discussed yet. Moreover, in most of these studies, radiative heat transfer was neglected or significantly simplified, because the computation of radiation further increases the computational cost. Watanabe et al. [5] studied the effects of radiation on the spray flame characteristics and soot formation by performing a two-dimensional DNS of spray flames formed in a laminar counterflow, in which the radiative interaction between the gas and dispersed droplets is taken into account, and found that the radiative heat transfer strongly affects the spray flame and soot formation behaviors. However, since the radiation effect is discussed only on the spray flames formed in a laminar counter flow, there remains uncertainty as to how the radiative heat transfer affects the characteristics of jet spray flames.

In LES and RANS (Reynolds-Averaged Navier-Stokes) simulations of gaseous combustions, flamelet models [e.g., 13,14] have been widely used as the turbulent combustion model. However, in the original flamelet model in which the energy equation is not solved in the physical space, not only the radiative heat transfer but also convective heat transfer between the gas and droplets for the spray combustion cannot be taken into account. Recently, Ihme and Pitsch [12] extended the flamelet/progress-variable approach [15] (referred to as FPV, in this paper) to account for the radiative

heat transfer, and investigated the effects of radiation on the gas temperature and NO formation on LES of Sandia flame D and a realistic aircraft engine. However, they considered the radiation only in the gas phase using the optically thin approximation [16] and still neglected the heat transfer between droplets and ambient fluid including radiation.

The purpose of this study is therefore to investigate the effects of equivalence ratio, fuel droplet size, ambient pressure and radiation on the spray combustion behavior by means of two-dimensional DNS of spray jet flames. In addition, FPV coupled with the radiation model, which can account for the heat transfer between droplets and ambient fluid including radiation, (referred to as EFPV, in this paper) is proposed and validated by comparing with the results using the direct combustion model based on the Arrhenius formation (referred to as ARF, in this paper). n-decane ($C_{10}H_{22}$) is used as liquid spray fuel, and the evaporating droplets' motions are tracked by the Lagrangian method. The radiative heat transfer is calculated using the discrete ordinate method [17] with S_8 quadrature approximation. The present paper provides the first part of two investigations. In this part 1, the effects of equivalence ratio, fuel droplet size and radiation on the spray combustion behavior are investigated. In addition, the validity of EFPV in various equivalence-ratio and fuel-droplet-size conditions and in the presence of the radiation are examined. In part 2 [18], the effect of ambient pressure on the spray combustion behavior and the validity of EFPV in high-pressure condition will be discussed. Originally, combustion models such as FPV are intended for use in connection with SGS models for LES or RANS of the carrier gaseous phase. However, in order to avoid discussion of the effect of the SGS contributions on numerical accuracy, a numerical method using fine resolution without the SGS models is chosen here. In these papers, we simply call this method DNS, regardless of the combustion model.

2. Numerical Simulation

2.1. Numerical methods for ARF and EFPV

In ARF, the Arrhenius formation is directly solved in the physical space as well as the flow field. In EFPV, on the other hand, the Arrhenius formation is solved in

generating a lookup table called flamelet library. Therefore, the detailed spray combustion behavior is investigated based on ARF, and the validity of EFPV is discussed by comparing with the results obtained by ARF.

The set of governing equations of the carrier gaseous phase and dispersed droplets phase for ARF and EFPV are described in our previous papers [3-7]. n-decane ($C_{10}H_{22}$) is used as liquid fuel, and the combustion reaction of the evaporated n-decane with oxygen is described by a one-step global reaction model [19] as

$$C_{10}H_{22} + \frac{31}{2}O_2 \rightarrow 11H_2O + 10CO_2. \tag{1}$$

In this study, the treatment of the radiative heat transfer for ARF is modified from Watanabe et al. [5]. Computation of radiative heat transfer tends to be much expensive due to procedure of estimating non-gray gas absorption coefficient and solving the radiation intensity balance equation. A common and straightforward way to account for radiation in gaseous flames is to ignore the radiation effect or to employ the optically thin approximation [16] which can effectively reduce the computational cost of solving the radiation intensity transport equation. Moreover, even in the optically thin approximation [16], most researchers use gray gas approximation because it is still very expensive to estimate non-gray gas absorption coefficient. In this study, in order to take into account the non-gray gas absorption coefficient, a tabulated library which is pre-computed and parameterized as a four-dimensional function by partial pressures of fuel, CO_2 and H_2O gases , P_F, P_{CO_2} and P_{H_2O}, and gas temperature, T, is employed. Namely, the local value of the Plank mean gas absorption coefficient of the medium, α, is determined by the interpolation among these four variables as

$$\alpha = \alpha(P_F, P_{CO_2}, P_{H_2O}, T). \tag{2}$$

More than 80 % of the computational cost for the total computation can be effectively reduced by the presented method. The value of α is calculated using a detailed narrow-band model RADCAL [20]. The radiative heat transfer is computed based on the discrete ordinate method [17]. For the standard FPV, the heat transfer between droplets and ambient fluid including radiation cannot be taken into account, as described earlier. Therefore, in the present EFPV, the total enthalpy is solved in the

physical space in order to account for the heat transfer between droplets and ambient fluid including radiation similarly to ARF and the gas temperature obtained from the flamelet library is corrected by

$$\Delta T = \frac{h - h_{lib}}{c_p}, \tag{3}$$

where h and h_{lib} are the total enthalpy obtained from the physical space and flamelet library, respectively. The details of the generation procedure of the flamelet library for this study is described in Baba and Kurose [6].

2.2. Computational details

The computational details adopted here are basically the same as our previous study [6]. Fig. 1 shows the schematic of the computational domain and inlet conditions. The length and velocity are non-dimensionalized by the reference length ($L_0 = 1.5 \times 10^{-2}$ m) and velocity ($U_0 = 15$ m s^{-1}), respectively. The dimensions of the computational domain are 5 and 2 in the streamwise and spanwise directions ($0 \leq x \leq 5$ and $-1 \leq y \leq 1$), respectively. The stoichiometric mixture gas is issued from the inlets of $0.060 < y < 0.075$ and $-0.075 < y < -0.060$ as coflows to stably ignite the flame, and air is issued from the other inlets. The stoichiometric mixture properties are obtained from the flamelet library. The inflow velocities of the air carring fuel droplets, coflow and outer air are set to be U= 1, 1, 0.2, respectively. The velocity perturbations based on continuous sine functions with a magnitude of 5 % are imposed in the inflow velocities of the air carring fuel droplets. The inflow gas temperature nondimensionalized by reference temperature ($T_0 = 300$ K) is set to be $T = 1$, except the inlets for the stoichiometric mixture gas. Reynolds number, Re, based on the jet width and velocity is 2250. The fuel droplets (spray) with a certain size distribution are injected from the central inlet of $-0.065 < y < 0.065$ with air. Initial droplet locations are randomly given at $x = 0$, and the velocities are set to be equivalent to the gas-phase velocities at the center of the droplets. The liquid properties of n-decane are obtained from Abramzon and Sirignano [21]. The boiling temperature of droplet is T_{BL} =447.7 K, the heat capacity is $c_L = 2520.5$ J kg^{-1} K^{-1} and the density is $\rho = 642$ kg m^{-3}. The

latent heat of droplet evaporation, L_V, is a function of the temperature which is given by $L_V = 3.958 \times 10^4 \ (619 - T_d)^{0.38}$ J kg^{-1}.

The computational domain is divided into 1000 (in the x direction) $\times$ 440 (in the y direction) non-uniform computational grid points, and fine resolution is given around the center of the stream lines (the finest resolution is 75 μm $\times$ 35 μm in the x and y directions, respectively). For a numerical approximation of the gas phase, discretization of the nonlinear terms of the momentum equations is derived from a fourth-order fully conservative finite difference scheme [22,23], while those of the scalars such as enthalpy and mass fractions are computed by QUICK scheme. Other differentials are approximated by a second-order finite difference method. A convective outflow condition is applied to the outflow boundary of the streamwise direction. The slip wall condition is applied to the spanwise direction. For the time advancement, the fractional step method and the second-order explicit Runge-Kutta method are used for the gas and dispersed droplet phases, respectively.

In this study, the effects of equivalence ratio, fuel droplet size and radiation are investigated based on the computations with ARF. The equivalence ratio, ϕ, based on the air flow rate issued at the center port is ranged from 0.4 to 10, and the the maximum value of the non-dimensional initial droplet diameter, D_{max}, is ranged from 1.3×10^{-3} to 6.7×10^{-3} (i.e., the actual droplet diameter is from 20 μm to 100 μm) under the condition that the minimum value of the non-dimensional initial droplet diameter, D_{min}, is fixed to be 6.7×10^{-5}. A homogeneous droplet diameter distribution is used as droplet size distribution. The computations with and without the radiation are performed. In addition, the validity of EFPV is examined by comparing with the results obtained by the computations with ARF. The CPU times for ARF4 in Table 1 (see below) in which 10,000 droplets are tracked with and without the radiation are about 120 h and 47 h for 50,000 steps on NEC: SX-8, respectively.

3. Results and discussion

3.1. Effects of equivalence ratio and fuel droplet size (without radiation)

Table 1 shows the equivalence ratio, ϕ, and the maximum value of non-dimensional initial droplet diameter, D_{max}, of the cases performed under the condition without the radiation in this study and the general features of these spray flames. The values at where ϕ and D_{max} intersect indicate the contributions of the premixed flame to the sum of the premixed and diffusion flames at a certain moment in the upstream ($0 \leq x \leq 0.5$) and downstream ($3.0 \leq x \leq 3.5$) regions, P_p, estimated by

$$P_p = \frac{\int \dot{\omega}_p(x,y)dxdy}{\int \dot{\omega}(x,y)dxdy}. \tag{4}$$

Here $\dot{\omega}_p$ and $\dot{\omega}$ are the reaction rates of the premixed flame and the sum of the premixed and diffusion flames (total reaction rate), respectively. In the table, "–" represents the condition where the flame is not kept or the computation cannot be performed due to the lack of memory (i.e., the flame failed to be caught in the conditions with low ϕ and large D_{max}, whereas the computation couldn't be performed in the conditions with high ϕ and small D_{max} because too many droplets are generated to be simulated), and "×" means that neither flame exists in the region. The details of the highlighted cases referred as to ARF1 - ARF4 and a dashed line will be discussed later. It is observed that the spray flame generally consists of both diffusion and premixed flames as also mentioned by previous studies [1-3,6], and that P_p is strongly affected by ϕ and D_{max}. In $\phi \leq 4$, P_p of the upstream region increases as ϕ and/or D_{max} decrease, whereas P_p of the downstream region decreases as ϕ decreases and/or D_{max} increases. In $6 \leq \phi$, in contrast, P_p of both the upstream and downstream regions increase as ϕ increases.

In order to clarify such effects of the equivalence ratio and fuel droplet size, four specific cases highlighted in Table 1, namely ARF1-ARF4 are investigated in detail. Fig. 2 shows the distributions of instantaneous droplet location, gas temperature, T, and flame index, FI. Here FI is a parameter, which is given as

$$FI = \nabla Y_F \cdot \nabla Y_O, \tag{5}$$

and identifies regions where premixed and diffusion flames are located [24]. Here Y_F

and Y_O are the mass fractions of fuel gas and oxidizer, respectively. FI is positive for a premixed flame and is negative for a diffusion flame.

The preferential concentration of fuel droplets due to turbulent organized motions is clearly observed in Fig. 2. It is also found that due to the droplet evaporation the fuel droplets vanish in the downstream region in ARF1, ARF2 and ARF3, whereas they remain in the downstream region only in ARF4. This is mainly because the smaller the droplet is, the faster the droplet vanishes. However, even for the same D_{max}, there appears an evident difference in the droplet lifetime between ARF1 and ARF2. This is considered due to the fact that the evaporation rate in ARF2 is tend to be lower than that in AFR1, since the evaporation in ARF2 is somewhat suppressed by the higher concentration of the evaporated fuel gas caused by the higher equivalence ratio, ϕ.

The high gas temperature region is found to change from jet center to outer jet edges regions as ϕ increases, and distributes in the region where the droplets do not exist. This is attributed to the facts that combustion reaction is suppressed by the extremely high local concentration of the evaporated fuel gas (i.e., lack of oxygen) and that the gas temperature is reduced by the heat transfer between the gas and droplets with lower temperature, which includes the effect of the evaporative heat loss [3]. For the same reason, as D_{max} increases, the gas temperature in the central downstream region tends to decrease, as can be seen by comparing ARF2 and ARF3.

Judging from the distributions of FI, diffusion flame is generally formed along with the upstream droplets-remaining regions (i.e., cluster of fuel droplets) and the jet edges, whereas premixed flame is formed mainly outside the diffusion flame along with the upstream droplets-remaining regions. It is also observed that the diffusion flame expands downstream as ϕ increases, and that the premixed flame becomes marked as D_{max} decreases. In particular, the premixed flame in ARF2 is widely distributed in the central region of the jet. The reason is considered that since the gas temperature around the fuel droplet cluster is relatively low, fuel gas and oxygen are well mixed before combustion reaction takes place. These trends of the contribution of the premixed and diffusion flames is quantitatively shown in Fig. 3, where the streamwise variations of time-averaged contribution of premixed flame, $\overline{P}_p(x)$, are plotted. Here $P_p(x)$ is given

by

$$P_p(x) = \frac{\int \dot{\omega}_p(x,y)dy}{\int \dot{\omega}(x,y)dy}. \tag{6}$$

It is found that the contribution of the premixed flame is generally lower than that of the diffusion flame, and that it clearly expands downstream with increasing ϕ and become marked with decreasing D_{max}. Furthermore, the trends of P_p shown in Table 1 are similarly explained. The reason why P_p of the upstream region increases as ϕ and/or D_{max} decrease and P_p of the downstream region decreases as ϕ decreases and/or D_{max} increases in $\phi \leq 4$ is attributed to the facts that the smaller the droplet is, the faster the evaporation is and that the diffusion flame develops on the jet edges as ϕ increases. On the other hand, the reason why P_p of both the upstream and downstream regions increase as ϕ increases in $6 \leq \phi$ is considered due to that the evolution of the diffusion flame on the jet edges is saturated and, in return, the evolution of the premixed flame is enhanced with increasing ϕ.

In order to further investigate the formation mechanism of the premixed and diffusion flames in the upstream region, the spanwise profiles of time-averaged reaction rate, $\overline{\dot{m}}_F$, mass fractions of fuel gas ($C_{10}H_{22}$) and oxygen (O_2), $\overline{Y}_F$ and $\overline{Y}_O$, at $x = 0.5$ in ARF1, ARF2, ARF3 and ARF4 are shown in Fig. 4. Here $\dot{m}_F$ is non-dimentionalized using U_0, L_0 and density of air ($\rho_0 = 1.17$ kg m^{-3}) and ' *pre*' and '*diff*' indicate the areas of the premixed and diffusion flames, respectively. The premixed flame occurs in the region where both fuel gas and oxygen simultaneously increase or decrease as y increases, whereas the diffusion flame occurs in the region where either of the fuel gas or oxygen increases and the other decreases as y increases. Accordingly, the premixed flame appears in the region between the top of fuel gas and the bottom of oxygen, and the diffusion flames appear on both sides of the premixed flame. Such premixed flame area tends to become large as the increase of fuel gas due to the droplet evaporation and/or the consumption of oxygen due to the chemical reaction are enhanced, that is, as ϕ increases and/or D_{max} decreases.

3.2. Performance of EFPV (without radiation)

The validity of EFPV is examined by comparing with the results using the direct combustion model based on ARF. The computations are performed for the same four

conditions as in the previous section (i.e., ARF1, ARF2, ARF3 and ARF4) and the corresponding cases are referred to as EFPV1, EFPV2, EFPV3 and EFPV4, respectively.

Fig. 5 shows the distributions of instantaneous gas temperature, T, in EFPV1, EFPV2, EFPV3 and EFPV4. The tendencies of the gas temperature distributions by EFPV are found to be similar to those by ARF (see Fig. 3). The high gas temperature region changes from jet center to outer jet edges as ϕ increases, and the gas temperature in the central downstream region decreases as D_{max} increases.

The comparisons of the spanwise profiles of time-averaged gas temperature, $\overline{T}$, and mixture fraction, $\overline{Z}$, at $x = 0.5$ and 3.0 between ARF and EFPV are shown in Figs. 6 and 7, respectively. For both $\overline{T}$ and $\overline{Z}$, the profiles by EFPV are observed to be in general agreement with those by ARF in all cases. However, there appear marked discrepancies in $\overline{T}$ in the central region between ARF2 and EFPV2, ARF3 and EFPV3, and ARF4 and EFPV4. That is, in the central region, the $\overline{T}$ profiles by EFPV tend to wave at $x = 0.5$, and indicate lower values than those by ARF at $x = 3.0$. To understand such temperature behavior, the comparisons of the streamwise profiles of time-averaged gas temperature, $\overline{T}$, mixture fraction, $\overline{Z}$, progress variable, $\overline{C}$, and mass fractions of fuel gas ($C_{10}H_{22}$) and oxygen (O_2), $\overline{Y}_F$ and $\overline{Y}_O$, between ARF2 and EFPV2 are shown in Fig. 8. It is found that in EFPV2 a sudden increase of $\overline{T}$ in the upstream region acts to disturb its continuous increase in the downstream region. These improbable temperature increases observed in the upstream region both on the spanwise and streamwise profiles are considered due to two inevitable deficits of the flamelet model, one of which is that the gas temperature obtained by the flamelet model indicates high values on both sides of the Z peak when the peak largely exceeds the stoichiometric value ($Z_{st} = 0.0625$ in this case). This is caused by the fact that the mixture fraction, Z, for the spray combustion is not the conserved scalar, as explained by Watanabe et al. [4]. The another deficit is that the flamelet model cannot precisely predict the ignition of the flame. That is, gas temperature is raised directly by ignition of high temperature gas in ARF, but it is raised through the flamelt library by the presence of the product mas fraction, i.e., progress variable C ($=Y_{CO_2} + Y_{H_2O}$) in

EFPV. This causes the quicker increase of the gas temperature in the upstream region in EFPV. In another words, it may be said that the flamelet model cannot predict the premixed flame appeared in the upstream region of the spray flame. In fact, in ARF2 where the premixed flame is most marked (see Fig. 2), the discrepancy in the gas temperature between ARF2 and EFPV2 is largest, since the combustion reaction in EFPV2 quickly takes place before the fuel gas and oxidizer are well mixed.

As described above, the improbable temperature increase in the upstream region deteriorates the performance of EFPV on spray flames. Therefore, it is useful to understand the conditions where it appears. In the aforementioned Table 1, the conditions on the right and left hand sides of a dashed line belong to the cases where the improbable temperature increase appear and does not appear, respectively. The improbable temperature increase in the upstream region is found to appear in the high ϕ conditions. Also, although the tendency is not shown in the Table, the improbable temperature increase tended to be remarkable as D_{max} decreases.

3.3. Effect of radiation

Fig. 9 shows the comparison of the spanwise profile of time-averaged gas temperature, $\overline{T}$, among ARF4, ARF4 with radiation (ARF4-R), EFPV4, and EFPV4 with radiation (EFPV4-R). Since the temperature difference is marked on the peak temperature, the difference is magnified in this figure. The comparison of ARF4 and ARF4-R shows that $\overline{T}$ in ARF4-R is lower than that in ARF4 on the peak value. The differences are approximately several decades of Kelvin. This is because the radiative heat transfer is affected by the existence of reaction products CO_2 and H_2O, whose absorption coefficients are relatively larger than those of other chemical species. It is also found that this radiation effect on $\overline{T}$ can be well predicted by EFPV4-R quantitatively. Moreover, although the result is omitted here, the comparison of the tome-averaged gas temperature profile between with and without the interaction of the gas and dispersed-droplets phaseshowed that the effect was largest in the upstream central region where many droplets exist but it was very small of several Kelvin (i.e., $Q_{rad,d}$ decreases the gas temperature by several Kelvin), and that the effect can be precisely captured by the present EFPV. Thus, it can be said that EFPV is a very useful model to capture the

spray combustion behavior including the effect of radiation. The similar tendencies of the radiation effect were observed in the other cases of ARF1-3.

4. Conclusions

The effects of equivalence ratio, fuel droplet size, and radiation on jet spray flames were investigated by means of two-dimensional direct numerical simulation (DNS). In addition, the validity of an extended flamelet/progress-variable approach (EFPV), in which heat transfer between droplets and ambient fluid including radiation was exactly taken into account, is examined. n-decane ($C_{10}H_{22}$) was used as liquid spray fuel, and the evaporating droplets' motions were tracked by the Lagrangian method. The radiative heat transfer was calculated using the discrete ordinate method with S_8 quadrature approximation. The main results obtained in this study can be summarized as follows.

(1) As equivalence ratio increases, high gas temperature region changes from jet center to outer jet edges, and diffusion flame expands downstream.

(2) As fuel droplet size increases, gas temperature in the central downstream region decreases, and premixed flame becomes marked.

(3) The behavior of the jet spray flames including the heat transfer between droplets and ambient fluid with radiation effect can be generally captured by EFPV. However, the accuracy tends to diminish as equivalence ratio increases and/or fuel droplet size decreases.

Acknowledges

The authors are grateful to Dr. Yuya Baba of Earth Simulator Center, Japan Agency for Marine-Earth Science Technology (JAMSTEC) and Mr. Yutaka Yano of Kyoto University for many useful discussions. A portion of this research was supported by the grant for "Strategic Program - Research Field No. 4: Industrial Innovations" from the Ministry of Education, Culture, Sports, Science, and Technology (MEXT)'s "Development and Use of Advanced, High-Performance, General-Purpose Supercomputers Project".

References

[1] Réveillon J, Vervisch L. Analysis of weakly turbulent dilute-spray flames and spray combustion regimes. J Fluid Mech 2005;537:317–347.

[2] Domingo P, Vervisch L, Réveillon J. DNS analysis of partially premixed combustion in spray and gaseous turbulent flame-bases stabilized in hot air. Combust Flame 2005;140:172–195.

[3] Nakamura M, Akamatsu F, Kurose R, Katsuki M. Combustion mechanism of liquid fuel spray in a gaseous flame. Phys Fluids 2005;17:123301.

[4] Watanabe H, Kurose R, Hwang S, Akamatsu F. Characteristics of flamelets in spray flames formed in a laminar counterflow. Combust Flame 2007;148:234–248.

[5] Watanabe H, Kurose R, Komori S, Pitsch H. Effects of radiation on spray flame characteristics and soot formation. Combust Flame 2008;152:2–13.

[6] Baba Y, Kurose R. Analysis and flamelet modelling for spray combustion. J Fluid Mech 2008;612:45–79.

[7] Hayashi J, Watanabe H, Kurose R, Akamatsu F. Effects of fuel droplet size on soot formation in spray flames formed in a laminar counterflow. Combust Flame 2011;158:2559-2568.

[8] Luo K, Pitsch H, Pai MG, Desjardins O. Direct numerical simulations and analysis of three-dimensional n-heptane spray flames in a model swirl burner. Proc Combust Inst 2011;33:2143–2152.

[9] Moin P, Apte SV. Large-eddy simulation of realistic gas turbine combustors. AIAA J 2006;44:698–708.

[10] Boileau M, Pascaud S, Riber E, Cuenot B, Gicquel LYM, Poinsot TJ, Cazalens M. Investigation of two-fluid methods for large eddy simulation of spray combustion in gas turbine. Flow Turb Combust 2008;80:291–321.

[11] Patel N. Menon S. Simulation of spray-turbulence-flame interactions in a lean direct injection combustor. Combust Flame 2008;53:228–257.

[12] Ihme M, Pitsch H. Modeling of radiation and nitric oxide formation in turbulent nonpremixed flames using a flamelet/progress variable formulation. Phys Fluids 2008;20:055110.

[13] Peters N. Laminar diffusion flamelet models in non-premixed turbulent combustion. Prog Energy Combust Sci 1984;10:319–339.

[14] Pitsch H, Steiner H. Large-eddy simulation of a turbulent piloted methane/air diffusion flame (Sandia flame D). Phys Fluids 2000;12:2541–2554.

[15] Pierce CD, Moin P. Progress-variable approach for large-eddy simulation of non-premixed turbulent combustion. J Fluid Mech 2004;504:73–97.

[16] Barlow RS, Karpetis AN, Frank JH, Chen JY. Scalar profiles and NO formation in laminar opposed-flow partially premixed methane/air flames. Combust Flame 2001;127:2102–2118.

[17] Fiveland WA. Three-dimensional radiative heat-transfer solutions by the discrete-ordinate method. J Thermophys 1988;2:309–316.

[18] Kitano T., Nakatani T., Kurose R., Komori S. Two-dimensional direct numerical simulation of spray flames. Part 2: Effects of ambient pressure and lift, and validity of flamelet model. Fuel, submitted.

[19] Westbrook CK, Dryer FL. Chemical kinetic modeling of hydrocarbon combustion. Prog Energy Combust Sci 1984;10:1–57.

[20] Grosshandler WL. RADCAL: A narrow-band model for radiation calculation in a combustion environment. NIST technical note 1993;1402.

[21] Abramzon B, Sirignano WA. Droplet vaporization model for spray combustion calculation. Int J Heat Mass Transfer 1989;32:1605–1618.

[22] Morinishi Y, Lund TS, Vasilyev OV, Moin P. Fully conservative higher order finite difference schemes for incompressible flow. J Compu Phys 1998;143:90–124.

[23] Nicoud F. Conservative high-order finite-difference schemes for low-Mach number flows. J Compu Phys 2000;158:71–97.

[24] Yamashita H, Shimada M, Takeno T. A numerical study on flame stability at the transition point of jet diffusion flames. Proc Combust Inst 1996;26:27–34.

NOMENCLATURE

C	progress variable, -
c_L	specific heat of liquid fuel, J kg^{-1} K^{-1}
c_p	specific heat of mixture gas, J kg^{-1} K^{-1}
D	non-dimensional initial droplet diameter, -
FI	flame inde0x, -
h	total enthalpy of mixture gas, J kg^{-1}
L	length, m
L_V	latent heat of droplet evaporation, J kg^{-1}
P_k	partial pressure of kth species, Pa
P_p	contribution of premixed flame, -
T	gaseous temperature, K
U	velocity, s^{-1}
Y_k	mass fraction of kth species, -
Z	mixture fraction, -
α	Plank mean gas absorption coefficient, m^{-1}
ϕ	equivalence ratio, -
ρ	density, kg m^{-3}
BL	boiling point
F	fuel gas
lib	flamelet library
max	maximum value
min	minimum value
O	oxidizer
0	reference value

LIST OF TABLE AND FIGURE

Table 1:

D_{max} \ ϕ	0.4	0.6	0.8	1.0	2.0	4.0	6.0	10.0
6.7×10^{-3}	–	–	–	–	–	–	9.45 : 4.32	12.8 : 4.43 (ARF4)
4.0×10^{-3}	–	–	–	–	11.5 : 7.24 (ARF3)	11.2 : 7.55	11.8 : 7.85	–
2.7×10^{-3}	–	–	14.5 : 0.00	14.1 : 0.00	13.0 : 17.7	11.8 : 32.5	–	–
2.0×10^{-3}	–	21.7 : 0.00 (ARF1)	20.0 : 0.00	18.2 : 0.00	16.9 : 22.2 (ARF2)	–	–	–
1.3×10^{-3}	40.5 : ×	35.6 : ×	32.6 : 0.00	30.8 : 0.00	20.5 : 22.8	–	–	–

without improbable temperature increase ← | → with improbable temperature increase

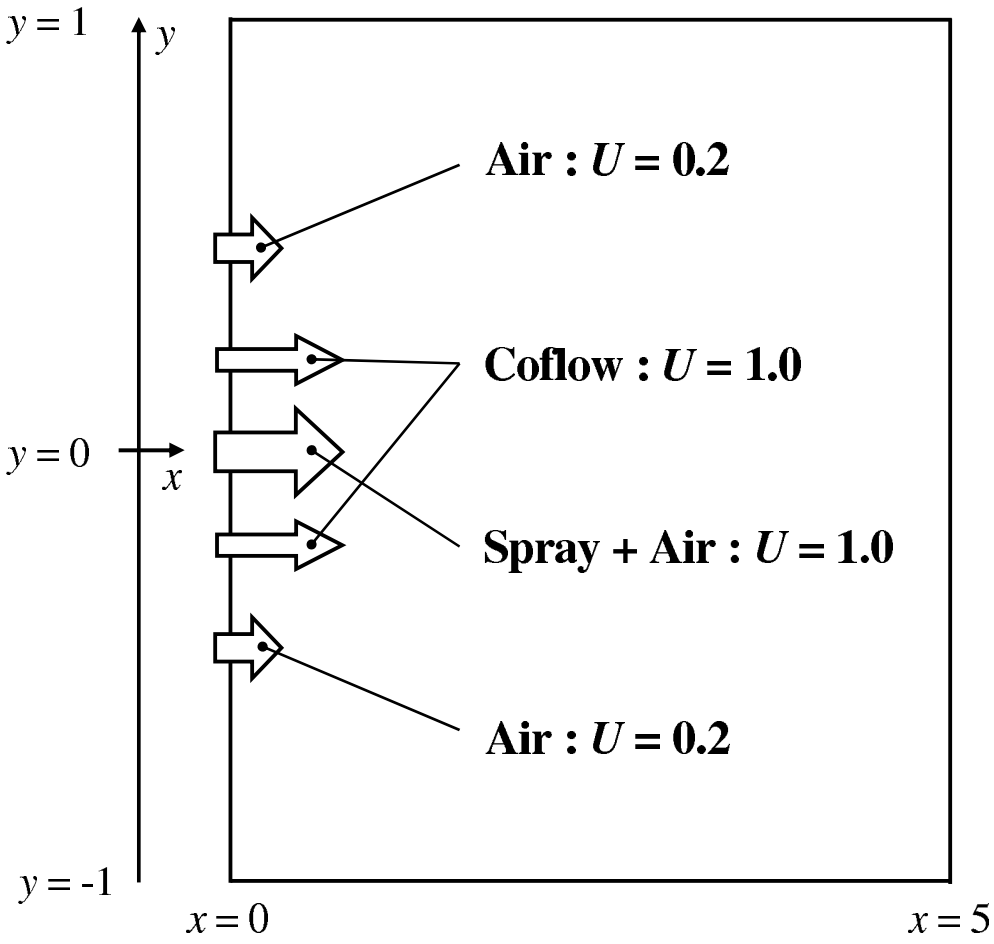

Figure 1:

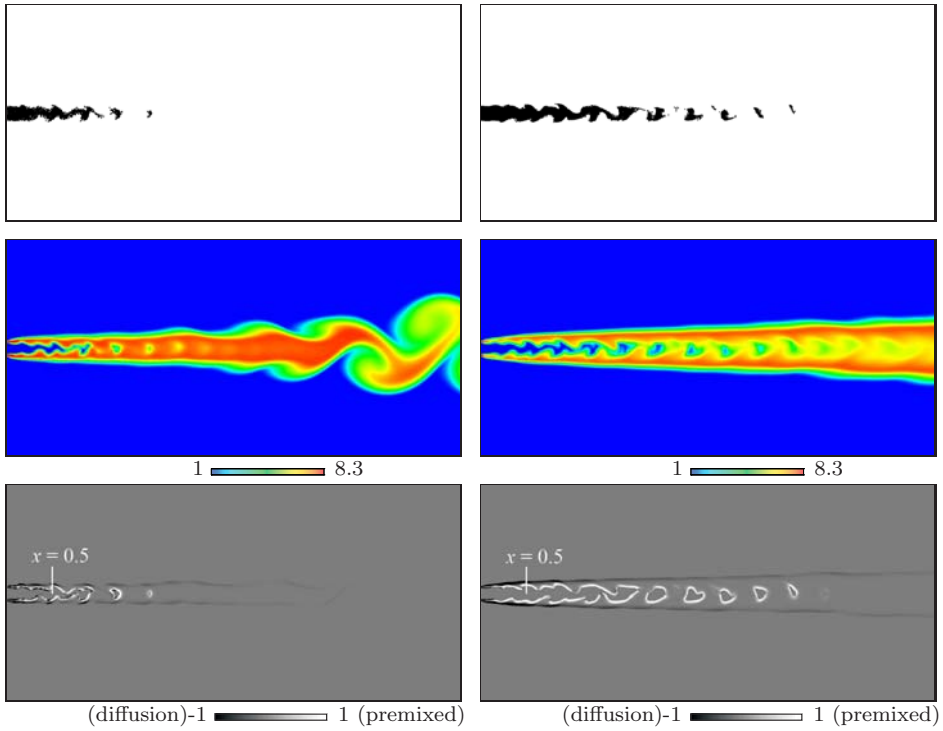

(a) (b)

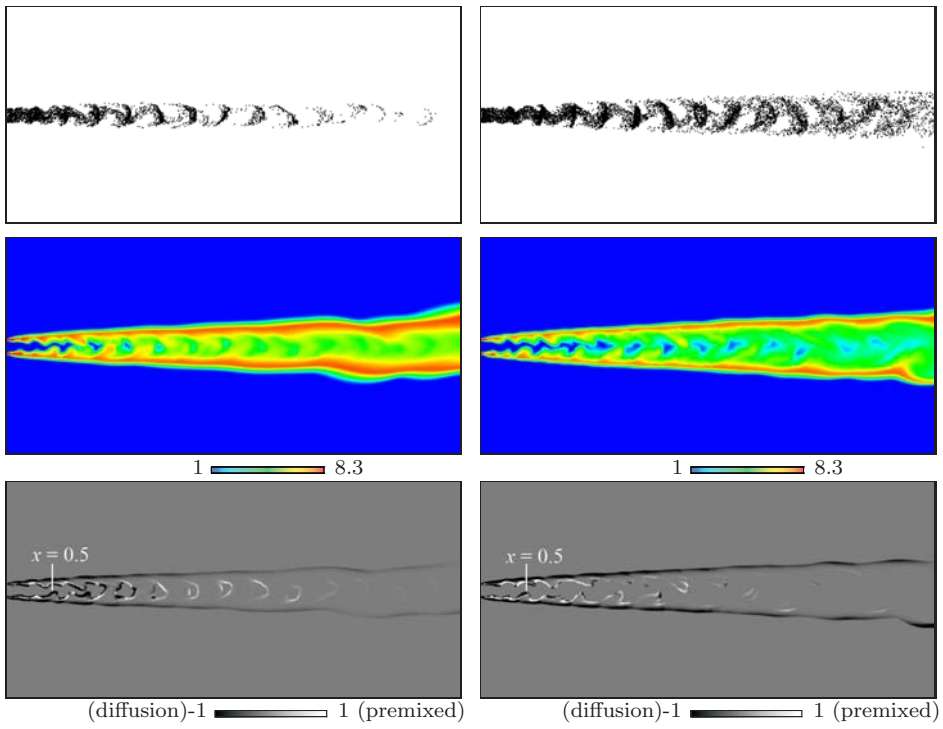

(c) (d)

Figure 2:

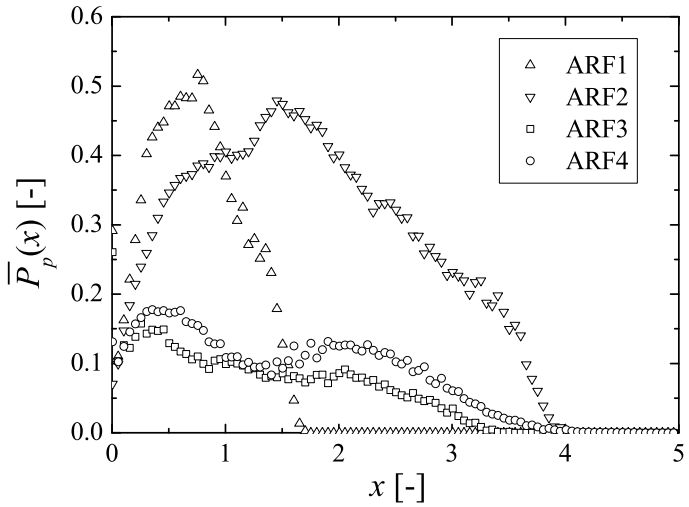

Figure 3:

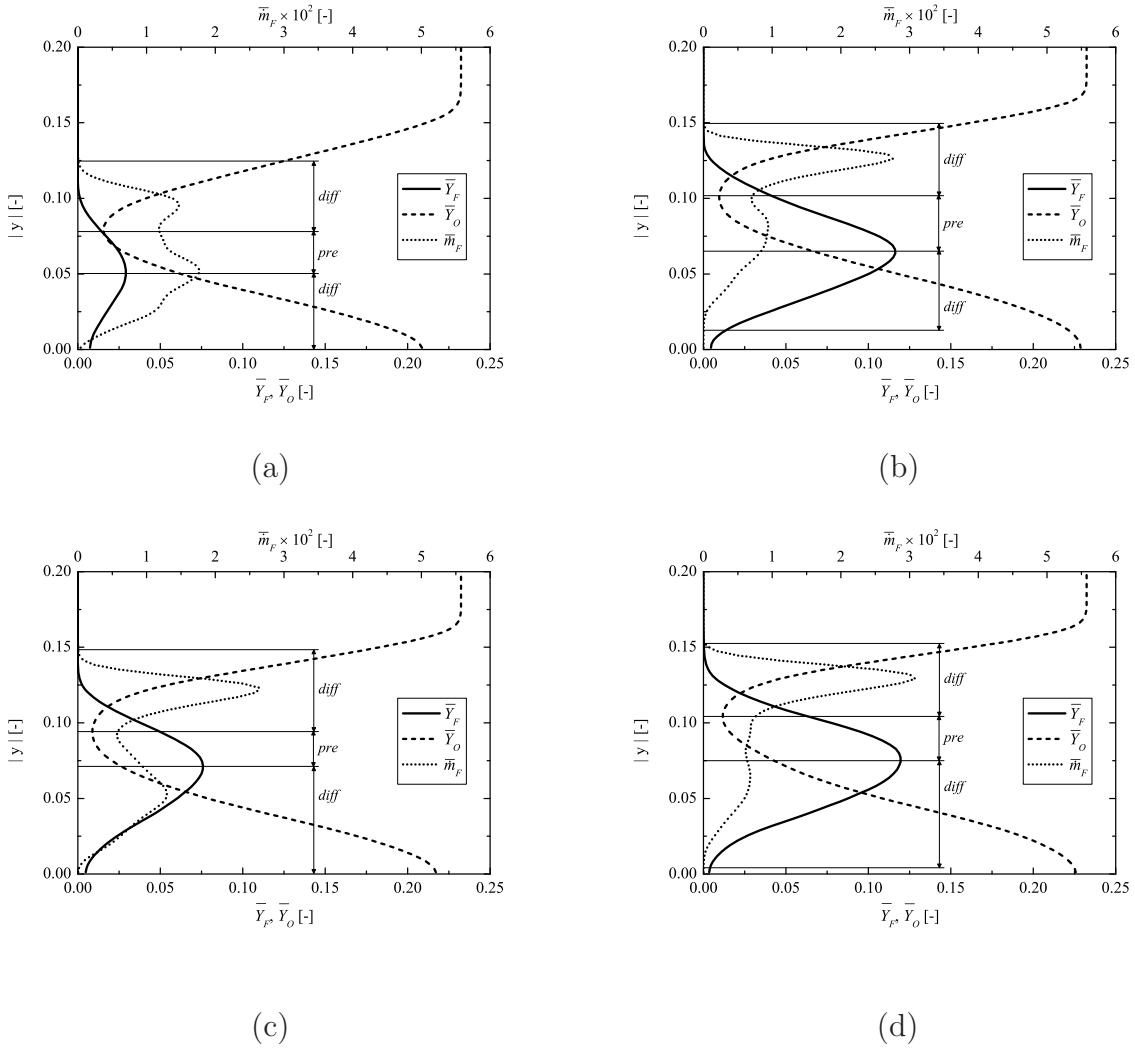

Figure 4:

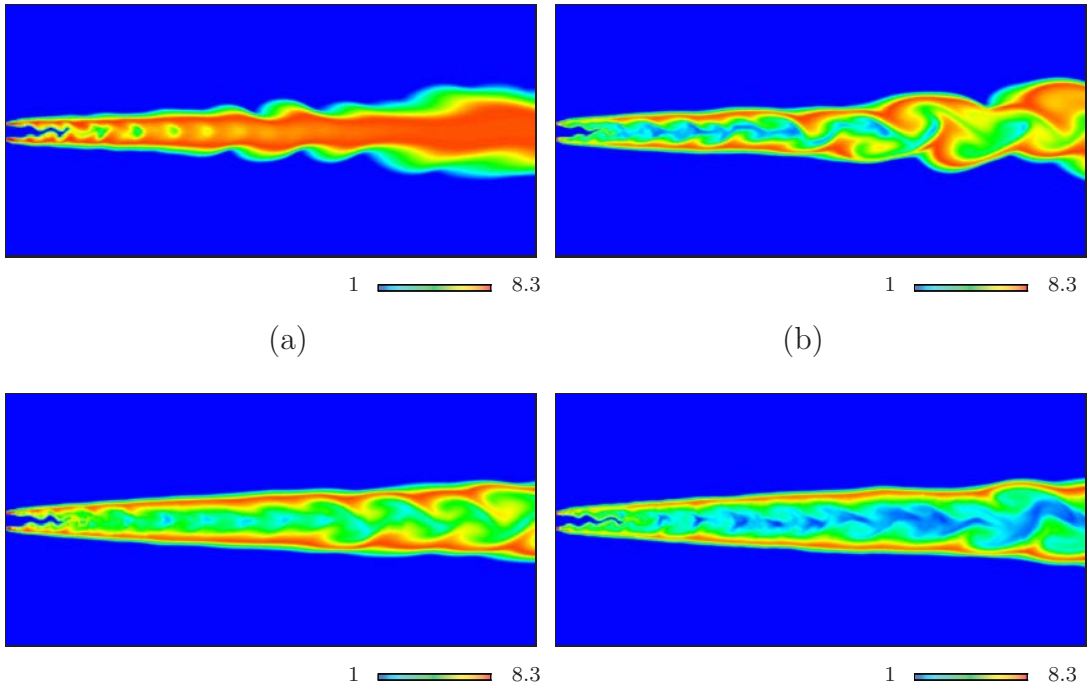

Figure 5:

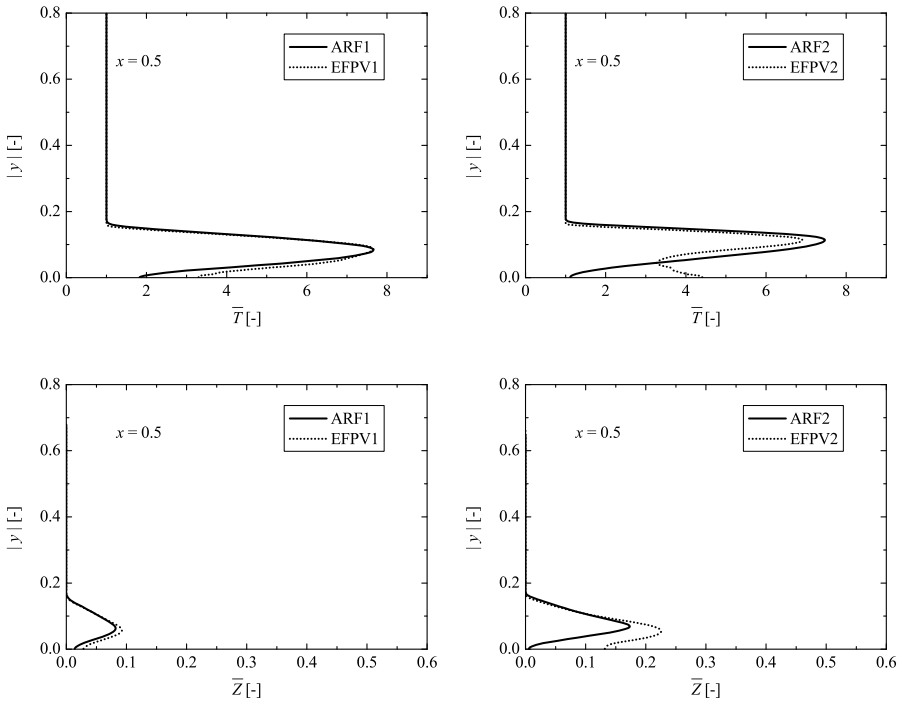

(a)

(b)

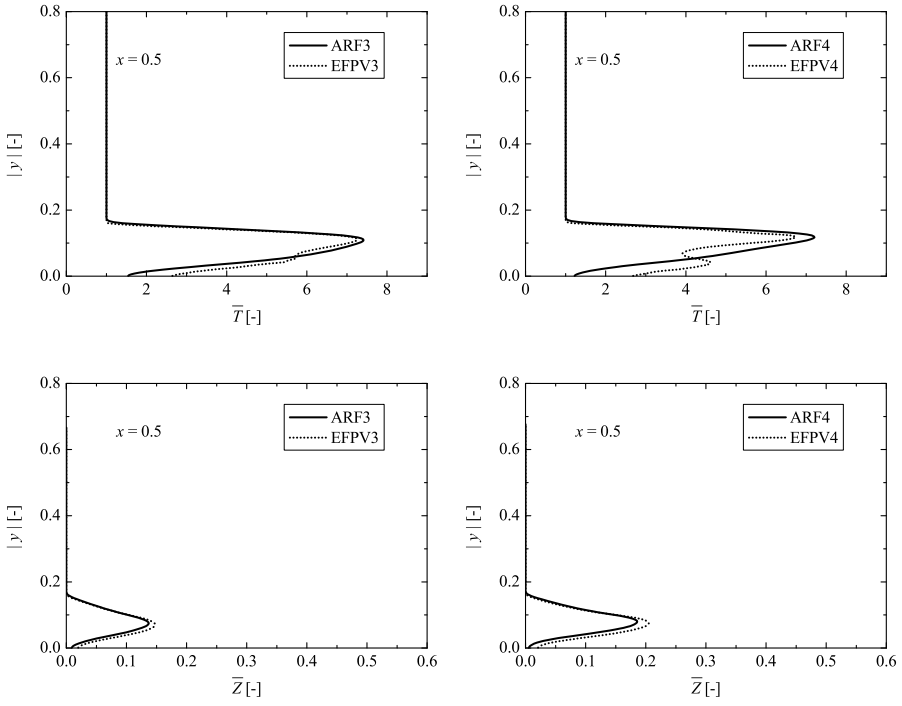

(c)

(d)

Figure 6:

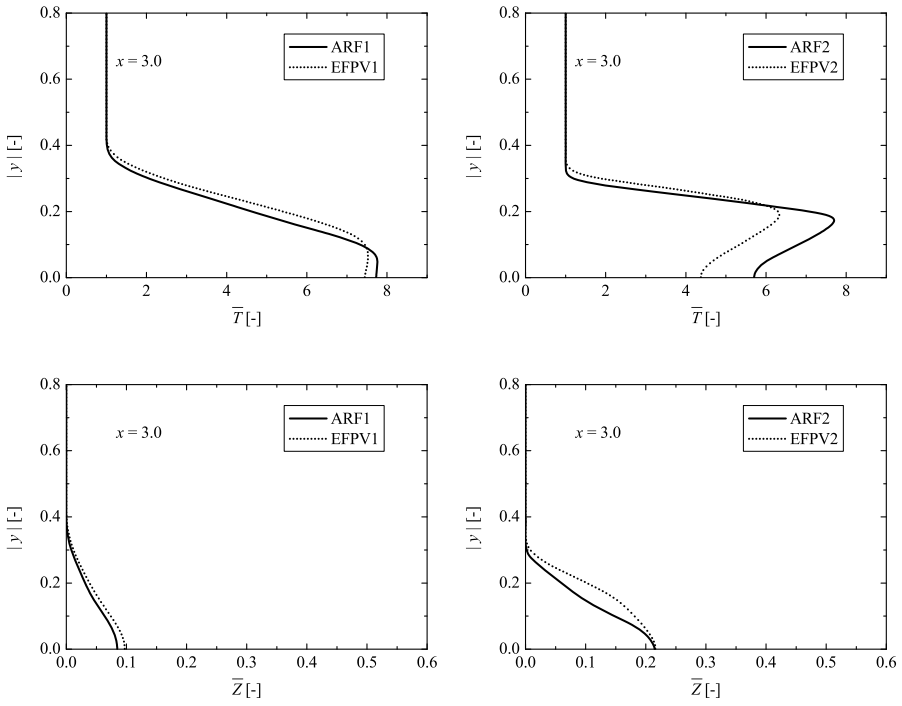

(a)

(b)

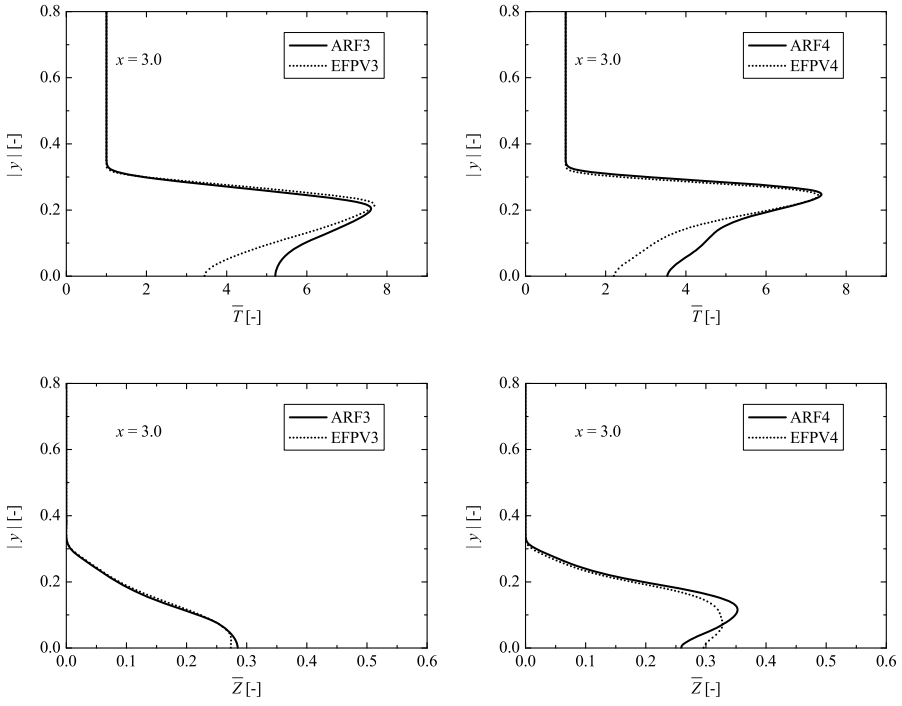

(c)

(d)

Figure 7:

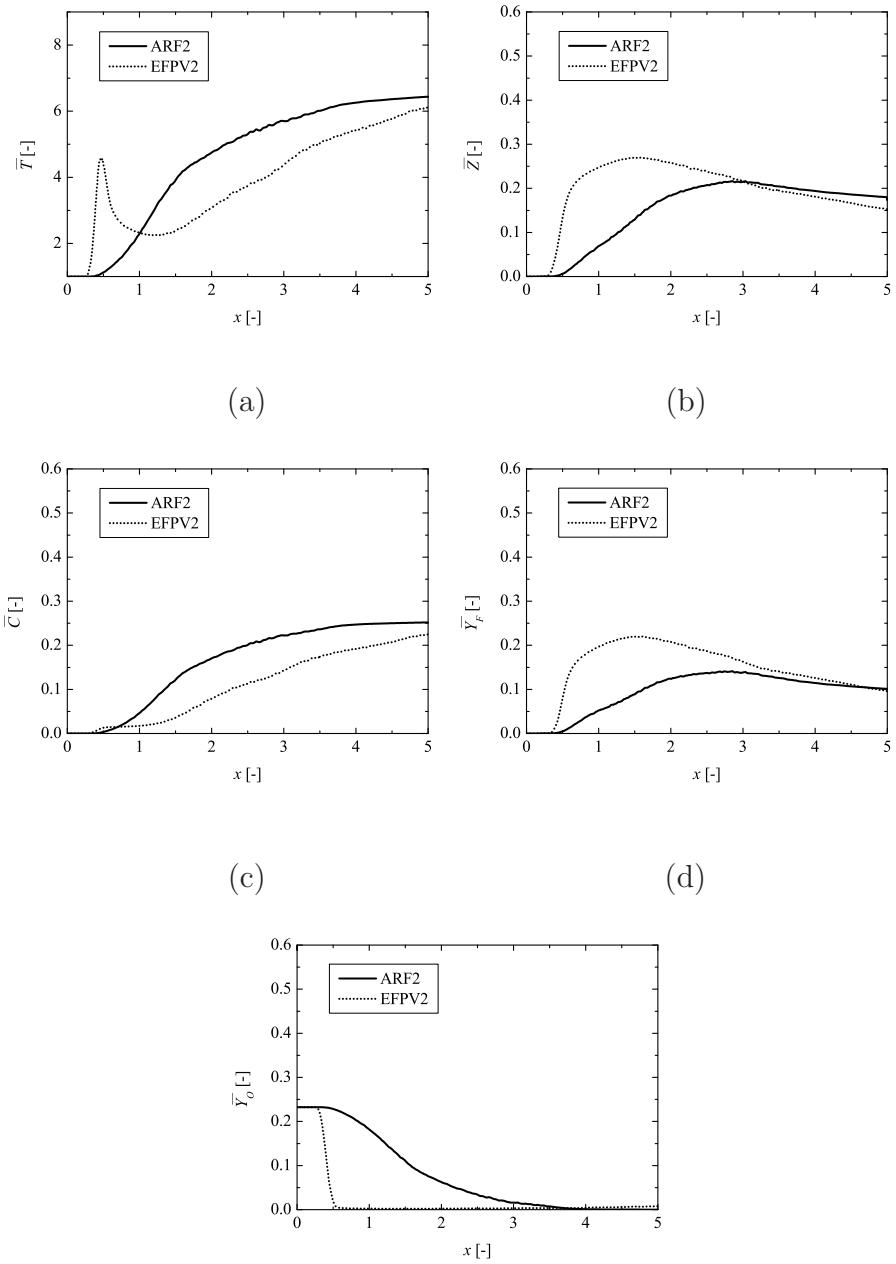

Figure 8:

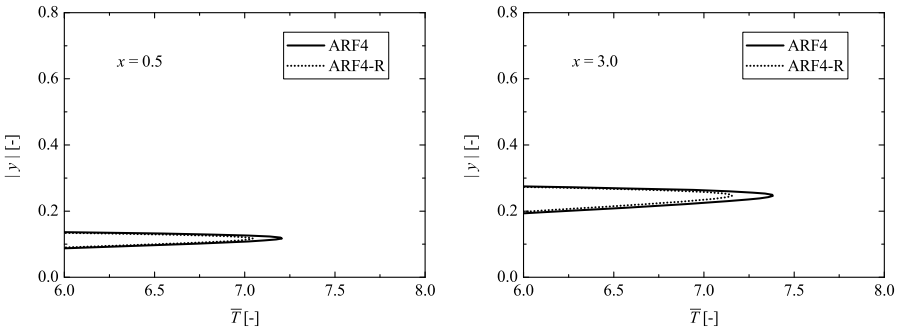

(a)

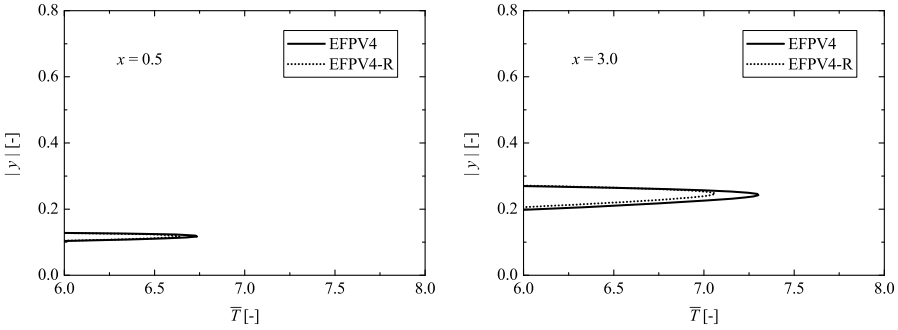

(b)

Figure 9: